Far-field scattering microscopy applied to analysis of slow light, power enhancement, and delay times in uniform Bragg waveguide gratings

W. C. L. Hopman, H. J. W. M. Hoekstra, R. Dekker, L. Zhuang, and R .M. de Ridder

Faculty of Electrical Engineering, Mathematics and Computer Science, Mesa+ Institute for Nanotechnology, University of Twente, PO Box 217, 7500AE Enschede, The Netherlands

Wico.Hopman@utwente.nl, R.M.deRidder@ewi.utwente.nl

Abstract: A novel method is presented for determining the group index, intensity enhancement and delay times for waveguide gratings, based on (Rayleigh) scattering observations. This far-field scattering microscopy (FScM) method is compared with the phase shift method and a method that uses the transmission spectrum to quantify the slow wave properties. We find a minimum group velocity of 0.04c and a maximum intensity enhancement of ~14.5 for a 1000-period grating and a maximum group delay of ~80 ps for a 2000-period grating. Furthermore, we show that the FScM method can be used for both displaying the intensity distribution of the Bloch resonances and for investigating out of plane losses. Finally, an application is discussed for the slow-wave grating as index sensor able to detect a minimum cladding index change of 10^{-8}, assuming a transmission detection limit of 10^{-4}.

OCIS codes: 290.5820 Scattering measurements; (230.5750) Resonators; (230.3990) Microstructure devices; (120.5820) Scattering measurements; (120.7000) Transmission; (130.3120) Integrated optics devices; 050.2230 Fabry-Perot; 050.2770 Gratings; 070.4790 Optical spectrum analysis; 110.3080 Infrared imaging; 260.5740 Resonance; 130.6010 Sensors

References and links

1. J. F. Lepage, R. Massudi, G. Anctil, S. Gilbert, M. Piche, and N. McCarthy, "Apodizing holographic gratings for the modal control of semiconductor lasers," Appl. Opt. **36**, 4993-4998 (1997).
2. W. C. L. Hopman, P. Pottier, D. Yudistira, J. van Lith, P. V. Lambeck, R. M. De La Rue, A. Driessen, H. Hoekstra, and R. M. de Ridder, "Quasi-one-dimensional photonic crystal as a compact building-block for refractometric optical sensors," IEEE J. Sel. Tops. Quantum Electron. **11**, 11-16 (2005).
3. P. Madasamy, G. N. Conti, P. Poyhonen, Y. Hu, M. M. Morrell, D. F. Geraghty, S. Honkanen, and N. Peyghambarian, "Waveguide distributed Bragg reflector laser arrays in erbium doped glass made by dry Ag film ion exchange," Opt. Eng. **41**, 1084-1086 (2002).
4. H. C. Wu, Z. M. Sheng, and J. Zhang, "Chirped pulse compression in nonuniform plasma Bragg gratings," Appl. Phys. Lett. **87**, 201502/1-3 (2005).
5. D. Pezzetta, C. Sibilia, M. Bertolotti, J. W. Haus, M. Scalora, M. J. Bloemer, and C. M. Bowden, "Photonic-bandgap structures in planar nonlinear waveguides: application to second-harmonic generation," J. Opt. Soc. Am. B **18**, 1326-1333 (2001).
6. D. Faccio, F. Bragheri, and M. Cherchi, "Optical Bloch-mode-induced quasi phase matching of quadratic interactions in one-dimensional photonic crystals," J. Opt. Soc. Am. B **21**, 296-301 (2004).
7. J. Ctyroky, S. Helfert, R. Pregla, P. Bienstman, R. Baets, R. De Ridder, R. Stoffer, G. Klaasse, J. Petracek, P. Lalanne, J. P. Hugonin, and R. M. De La Rue, "Bragg waveguide grating as a 1D photonic band gap structure: COST 268 modelling task," Opt. Quantum Electron. **34**, 455-470 (2002).
8. J. D. Joannopoulos, R. D. Meade, and J. N. Winn, *Photonic crystals: Molding the flow of light* (Princeton University Press, 1995).
9. M. Soljacic, and J. D. Joannopoulos, "Enhancement of nonlinear effects using photonic crystals," Nat. Mater. **3**, 211-219 (2004).
10. V. I. Kopp, B. Fan, H. K. M. Vithana, and A. Z. Genack, "Low-threshold lasing at the edge of a photonic stop band in cholesteric liquid crystals," Opt. Lett. **23**, 1707-1709 (1998).

#78260 - $15.00 USD Received 20 December 2006; revised 8 February 2007; accepted 9 February 2007

11. A. Figotin, and I. Vitebskiy, "Slow light in photonic crystals," Waves Random Complex Media **16**, 293-382 (2006).
12. H. J. W. M. Hoekstra, W. C. L. Hopman, J. Kautz, R. Dekker, and R. M. de Ridder, "A simple coupled mode model for near band-edge phenomena in grated waveguides," accepted for publication in Opt. Quantum Electron. (2006).
13. W. C. L. Hopman, R. Dekker, D. Yudistira, W. F. A. Engbers, H. J. W. M. Hoekstra, and R. M. De Ridder, "Fabrication and characterization of high-quality uniform and apodized Si_3N_4 waveguide gratings using laser interference lithography," IEEE Photon. Technol. Lett. **18**, 1855-1857 (2006).
14. J. M. Bendickson, J. P. Dowling, and M. Scalora, "Analytic expressions for the electromagnetic mode density in finite, one-dimensional, photonic band-gap structures," Phys. Rev. E **53**, 4107-4121 (1996).
15. H. Gersen, T. J. Karle, R. J. P. Engelen, W. Bogaerts, J. P. Korterik, N. F. van Hulst, T. F. Krauss, and L. Kuipers, "Real-space observation of ultraslow light in photonic crystal waveguides," Phys Rev Lett **94** (2005).
16. C. E. Finlayson, F. Cattaneo, N. M. B. Perney, J. J. Baumberg, M. C. Netti, M. E. Zoorob, M. D. B. Charlton, and G. J. Parker, "Slow light and chromatic temporal dispersion in photonic crystal waveguides using femtosecond time of flight," Phys. Rev. E **73**, 016619/1-10 (2006).
17. R. S. Jacobsen, A. V. Lavrinenko, L. H. Frandsen, C. Peucheret, B. Zsigri, G. Moulin, J. Fage-Pedersen, and P. I. Borel, "Direct experimental and numerical determination of extremely high group indices in photonic crystal waveguides," Opt. Express. **13**, 7861-7871 (2005).
18. M. C. Netti, C. E. Finlayson, J. J. Baumberg, M. D. B. Charlton, M. E. Zoorob, J. S. Wilkinson, and G. J. Parker, "Separation of photonic crystal waveguides modes using femtosecond time-of-flight," Appl. Phys. Lett. **81**, 3927-3929 (2002).
19. Y. A. Vlasov, S. Petit, G. Klein, B. Honerlage, and C. Hirlimann, "Femtosecond measurements of the time of flight of photons in a three-dimensional photonic crystal," Phys. Rev. E **60**, 1030-1035 (1999).
20. Y. A. Vlasov, M. O'Boyle, H. F. Hamann, and S. J. McNab, "Active control of slow light on a chip with photonic crystal waveguides," Nature **438**, 65-69 (2005).
21. M. Notomi, K. Yamada, A. Shinya, J. Takahashi, C. Takahashi, and I. Yokohama, "Extremely large group-velocity dispersion of line-defect waveguides in photonic crystal slabs," Phys. Rev. Lett. **87**, 253902/1-4 (2001).
22. X. Letartre, C. Seassal, C. Grillet, P. Rojo-Romeo, P. Viktorovitch, M. Le Vassor D'Yerville, D. Cassagne, and C. Jouanin, "Group velocity and propagation losses measurement in a single-line photonic-crystal waveguide on InP membranes," Appl. Phys. Lett. **79**, 2312-2314 (2001).
23. K. Daikoku, and A. Sugimura, "Direct measurement of wavelength dispersion in optical fibres-difference method," Electron. Lett. **14**, 149-151 (1978).
24. K. Hosomi, T. Fukamachi, T. Katsuyama, and Y. Arakawa, "Group delay of a coupled-defect waveguide in a photonic crystal," Opt. Rev. **11**, 300-302 (2004).
25. S. Ryu, Y. Horiuchi, and K. Mochizuki, "Novel chromatic dispersion measurement method over continuous Gigahertz tuning range," J. Lightwave Technol. **7**, 1177-1180 (1989).
26. W. Bogaerts, P. Bienstman, D. Taillaert, R. Baets, and D. De Zutter, "Out-of-plane scattering in 1-D photonic crystal slabs," Opt. Quantum Electron. **34**, 195-203 (2002).
27. R. Ferrini, R. Houdre, H. Benisty, M. Qiu, and J. Moosburger, "Radiation losses in planar photonic crystals: two-dimensional representation of hole depth and shape by an imaginary dielectric constant," J. Opt. Soc. Am. B **20**, 469-478 (2003).
28. S. J. McNab, N. Moll, and Y. A. Vlasov, "Ultra-low loss photonic integrated circuit with membrane-type photonic crystal waveguides," Opt. Express. **11**, 2927-2939 (2003).
29. M. Loncar, D. Nedeljkovic, T. P. Pearsall, J. Vuckovic, A. Scherer, S. Kuchinsky, and D. C. Allan, "Experimental and theoretical confirmation of Bloch-mode light propagation in planar photonic crystal waveguides," Appl. Phys. Lett. **80**, 1689-1691 (2002).
30. D. J. W. Klunder, F. S. Tan, T. Van der Veen, H. F. Bulthuis, G. Sengo, B. Docter, H. J. W. M. Hoekstra, and A. Driessen, "Experimental and numerical study of SiON microresonators with air and polymer cladding," J. Lightwave Technol. **21**, 1099-1110 (2003).
31. D. B. Hunter, M. E. Parker, and J. L. Dexter, "Demonstration of a continuously variable true-time delay beamformer using a multichannel chirped fiber grating," IEEE Trans. Microwave Theory Tech. **54**, 861-867 (2006).
32. J. T. Hastings, M. H. Lim, J. G. Goodberlet, and H. I. Smith, "Optical waveguides with apodized sidewall gratings via spatial-phase-locked electron-beam lithography," J. Vac. Sci. Technol., B **20**, 2753-2757 (2002).
33. J. F. Lepage, and N. McCarthy, "Analysis of the diffractional properties of dual-period apodizing gratings: theoretical and experimental results," Appl. Opt. **43**, 3504-3512 (2004).
34. D. Wiesmann, C. David, R. Germann, D. Emi, and G. L. Bona, "Apodized surface-corrugated gratings with varying duty cycles," IEEE Photon. Technol. Lett. **12**, 639-641 (2000).
35. L. Xuhui, C. Xiangfei, Y. Yuzhe, and X. Shizhong, "A novel apodization technique of variable duty cycle for sampled grating," Opt. Commun. **225**, 301-305 (2003).
36. H. G. Winful, "The meaning of group delay in barrier tunnelling: A re-examination of superluminal group velocities," New J. Phys. **8**, 101/1-16 (2006).
37. Olympios, "OlympIOs Integrated Optics Software," C2V, http://www.c2v.nl/software/.
38. C. De Angelis, F. Gringoli, M. Midrio, D. Modotto, J. S. Aitchison, and G. F. Nalesso, "Conversion efficiency for second-harmonic generation in photonic crystals," J. Opt. Soc. Am. B **18**, 348-351 (2001).

#78260 - $15.00 USD Received 20 December 2006; revised 8 February 2007; accepted 9 February 2007

39. M. L. Povinelli, S. G. Johnson, and J. D. Joannopoulos, "Slow-light, band-edge waveguides for tunable time delays," Opt. Express. **13**, 7145-7159 (2005).
40. D. Yudistira, H. Hoekstra, M. Hammer, and D. Marpaung, "Slow light excitation in tapered 1D photonic crystals: Theory," Opt. Quantum Electron. **38**, 161-176 (2006).
41. P. V. Lambeck, "Integrated optical sensors for the chemical domain," Meas. Sci. Technol. **17**, R93-R116 (2006).

1. Introduction

Bragg waveguide gratings can be used in many integrated optical architectures to achieve a broad range of functionalities. For many years, they have for example shown their value in filters and mirrors [1], sensors [2], lasers [3], pulse compression [4], second harmonic generation [5, 6] and many more applications and theoretical studies. A waveguide grating (WGG) can be formed by periodic variation of the dielectric constant along the propagation direction. A straightforward method to achieve this modulation is by etching slits into a waveguide. The waveguide is needed for vertical and lateral confinement. WGGs having a strong modulation in dielectric constant, are often referred to as one-dimensional (1D) photonic crystals [7].

The 1D periodicity induces a gap in guided modes, the so-called photonic stop band. The corresponding dispersion curves of such a system reveal a slowdown of the group velocity near the band edges of the "semi-infinite" photonic crystal (PhC) [8]. In principle the theory shows that the group velocity approaches to zero at the band edges. This phenomenon is referred to as slow light in this paper; however the phase velocity still is in the order of the speed of light in vacuum, *c*. A slow light wave has a longer interaction time with the material it is traveling through. This effect can be exploited for example for sensors [2], nonlinear optical devices [9] and enhanced effective gain or low-threshold lasing [10]. However, a slow wave, or in the extreme a standing wave, can occur only over a very limited frequency range [11] which makes it unsuitable for high bandwidth-demanding telecom applications.

In finite periodic structures, the limited length causes characteristic fringes in the transmission and reflection spectra of WGGs, occurring near the band edge [12, 13] due to Fabry-Perot resonances of the grating Bloch modes [6]. The Fabry-Perot effect and the slow-wave effect are inseparable in such structures [12]. A maximum in the density of modes is found at the first resonant fringe [14] and not at the corresponding stop band edge positions of the equivalent infinite structure. The reflected power of Fabry-Perot-like resonators is generally minimum at the resonance wavelength [7]. However a fabricated structure may show increased loss at the resonance wavelength(s) because of out of plane scattering (OPS) and linear absorption, which are proportional to the field intensity. The scattering is caused by non-uniformities of the material and surface roughness due to etching processes.

Several measurement and analyzing methods have been proposed and applied for determining the group velocity or the group delay of a slow light wave in micrometer-sized devices. Examples are photon scanning tunneling microscopy (PSTM) [15], time of flight measurement [16-19], integrated Mach-Zehnder interferometers (MZI) [20], and spectral analysis of Fabry-Perot-like transmission phenomena [21, 22]. The major disadvantage of the present methods is that they are complex and time-consuming (time of flight and PSTM) or may demand special extra design complexity, as for example in the MZI-type measurements. The analysis of the Fabry-Perot like transmission phenomena is based on fitting calculated fringe locations (based on the Fabry-Perot free spectral range formula) to the measured spectrum, to obtain the group velocity as a fitting parameter. The approach uses a linear approximation of the dispersion, which results in the substitution of the phase index by the group index. This however affects the accuracy, because near the stop band edge the dispersion curve shows a strong curvature [12], resulting in a strong change in effective and group index near the stopband edge as we will show experimentally.

In this paper we introduce an alternative method –the far-field scattering (FScM) method– for estimating the power enhancement factor within the resonator, the group delay, and the resulting group index. The major advantage of our method, compared to the previously mentioned ones, is that analyzing the scattering intensity by infrared camera is an easy and

#78260 - $15.00 USD Received 20 December 2006; revised 8 February 2007; accepted 9 February 2007

straightforward technique for determining the group velocity at different wavelengths. We will demonstrate the quality of this method, by comparing its results to reference delay measurements using an interferometric setup, and by rigorous modeling. The only requirement for the method to work is that the device should show detectable randomly distributed scattering, which usually is not a problem.

We will first briefly present the design and fabrication of the characterized structures; a more detailed description of the fabrication method can be found elsewhere [13]. The scattering measurement setup is discussed in detail in section 3. A brief description of the setup used for reference delay measurements will also be given. In section 4 we present both the theory and simulations describing the resonance properties of the WGGs, and the experimental results obtained from the fabricated structures. In subsection 4.1 we will derive a relation for the group delay using the quality factor Q and also using the far-field scattering microscopy method. The modeling of the WGGs is presented in subsection 4.2 for verification of experimental results presented in subsection 4.3. In this subsection we will present our main experimental results, demonstrating Q factors up to 10^5, and showing how the "scatter-intensity" approach can be applied to slow-wave structures for estimating the corresponding group velocity. The results are verified with those obtained using the well-known RF phase shift method [17, 23-25]. In section 5 we will demonstrate how our method can be used to determine and study the OPS loss [26, 27]. In section 6 we discuss the application of slow light in WGGs for refractometric sensors, and the maximum sensitivity that can be achieved with such devices (10^{-8}). Finally we will present the main conclusions of this research in section 7.

2. Design and fabrication

A schematic 3D drawing of the WGG design is shown in Fig. 1(a), a SEM photo zoomed in on the grating, is shown in Fig. 1(b). The WGG was fabricated using a three-step etching process performed on a Si_3N_4 guiding layer with refractive index n = 1.981 and initial thickness d_g= 275 nm, which was LPCVD-deposited on top of a 9 micrometer thick SiO_2 (n = 1.445) buffer layer.

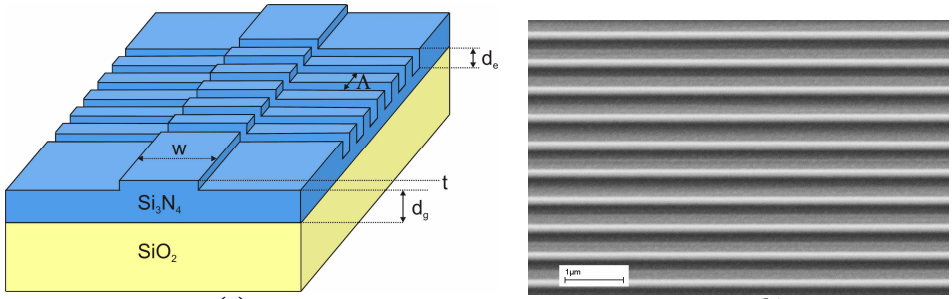

Fig. 1. (a). Schematic 3D drawing of the WGG. (b) Top view SEM image of a zoomed in view of the 500-Period WGG, the small ridge of only 5 nm is not observed in the image.

A small ridge-step t = 5 nm was chosen for lateral confinement. The advantage of the resulting small lateral effective index contrast is that a 2D model provides sufficient accuracy for designing the grating and simulating its optical properties [7]. Because of this contrast, a relatively large width w = 7 μm could be chosen for the ridge waveguide to be still single moded. In order to have a stop band in the 1.5 μm wavelength region, we chose the period of the WGGs to be Λ = 0.47 μm. The gratings were defined using laser interference lithography. After reactive ion etching of the grating mask the etch depth was estimated to be d_e = 50 nm (i.e. ~19 % of the core-thickness), using both profilometry and fitting of the measurement data using a mode expansion technique in 2D. The gratings were characterized with both an air cladding (n = 1) and a polymer cladding ($n \cong 1.5$) on top. In this paper we consider three

#78260 - $15.00 USD Received 20 December 2006; revised 8 February 2007; accepted 9 February 2007

different lengths of the WGGs, determined by the number of periods: 500, 1000 and 2000 periods. Further details of the fabrication process of similar WGGs can be found in [13].

3. Measurement setup

The WGGs were characterized using an end-fire setup, suitable for simultaneously obtaining the transmission spectrum and near infrared (NIR) scattered power images. This type of setup has proven its value in other applications such as determining the loss in a photonic crystal waveguide [28], characterization of apodized gratings [13], Bloch mode detection in photonic crystal waveguides [29], and mapping of the intracavity power of a micro-ringresonator [30]. A schematic drawing of the setup is depicted in Fig. 2. The highly linear and sensitive NIR-CCD-camera was positioned to collect scattered photons from the selected area, indicated by the (white) dotted area in Fig. 2. The camera produces 320 x 240 pixel images with a 12-bits pixel depth, where at the highest magnification each pixel represents the scattering from a 0.8 μm x 0.8 μm chip area.

By tuning the wavelength of the laser (λ_s), we obtain "scatter images" for each selected wavelength. The wavelength dependent scattering intensities of the selected area (region of interest: ROI) could be obtained by image processing of the scatter data. A tunable laser (HP 8186c) in combination with a polarization controller was used to couple light into the TE_{00} waveguide mode. The light source provided a wavelength range of 1470 nm to 1600 nm with a resolution of 1 pm. The transmission spectra of the waveguide gratings were normalized with respect to that of a reference waveguide without a grating, in order to cancel out any other wavelength dependencies in the optical path.

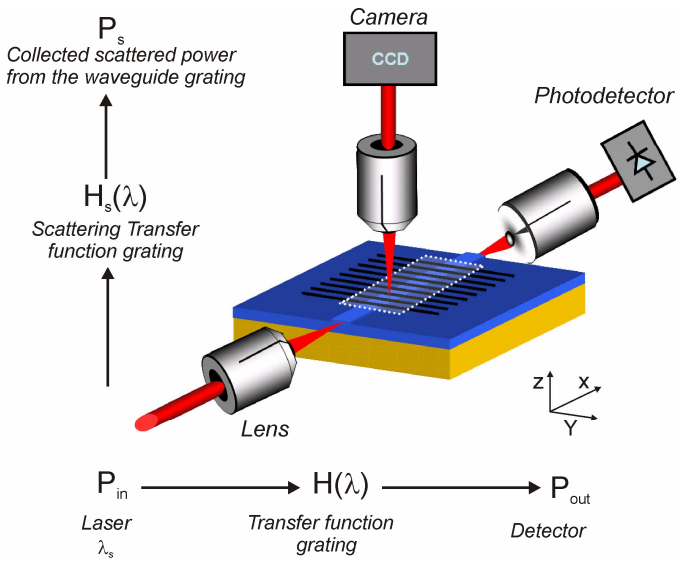

Fig. 2. Schematic drawing of the dual-setup: NIR CCD-camera + end-fire detection.

In principle all fabricated devices scatter due to inhomogenities in the waveguide structures. The scatterers obtained in our fabrication process have a random distribution, so that no coherent interference effects are to be expected. The size of the scatters is on average smaller than 50 nm (determined from the SEM images), well in the Rayleigh scattering regime for the considered wavelength range. For sufficiently low power, nonlinear effects can be neglected and the scattered intensity is directly proportional to the local light intensity in the structure. In practice our method is dependent on the (inevitable) fabrications errors in the device, the minimum detection level of the linear camera, and the materials used for realizing the waveguide gratings (WGGs). We estimate guiding losses due to imperfections of <8 dB/cm

#78260 - $15.00 USD Received 20 December 2006; revised 8 February 2007; accepted 9 February 2007

for the WGGs (at the reference wavelength), which is relatively low considering the strong corrugation. For the feeding waveguides we estimate a guiding loss of <1 dB/cm.
Nevertheless, the method is expected to work for even smoother WGGs (with lower loss) as well. We used a relatively low input power of 0.2 mW to avoid overexposure of the NIR camera. The input power can easily be increased by a factor of 10 if needed. Another increase in power of at least 10 can be achieved by optimizing the input and output coupling, i.e. replacing the objectives by for example small-core fibers and/or carefully optimizing the fiber-chip coupling in the design. Furthermore, the signal to noise level can also be increased by averaging multiple frames. We expect that by applying the aforementioned optimizations our method will also work for imperfection levels at least 100 times lower than in our WGG. Therefore, the method may yield accurate results for gratings with propagation losses due to scattering as small as 0.08 dB/cm.
The reference delay measurements were performed using an RF vector network analyzer (VNA) [31]. The phase of a 2 GHz RF modulation of the optical wave was measured with the VNA. From this phase shift the group delay, and hence the group velocity of the optical signal could be deduced. One erbium-doped fiber amplifier (+20 dB) was placed after the RF modulator and the another one was placed before the RF detector to amplify the power coupled into the device under test in order to obtain an as high as possible signal to noise ratio, while taking care not to excite nonlinear effects in the device.

4. Resonances in waveguide gratings

As already mentioned, the resonances in finite WGGs give rise to fringes in the transmission spectrum near the stopband edges. These alternating transmission maxima and minima are often unwanted, because they limit the available bandwidth, making the devices less suitable for high speed telecom optics. Reduction of these fringes through apodization has therefore been the subject of many investigations [13, 32-35]. The presence of the fringes in the transmission spectrum can be explained by longitudinal resonances which occur due to interference of the Bloch harmonics in the structure [6, 11, 12], with each maximum corresponding to a specific intensity distribution along the WGG. This phenomenon is studied here numerically and experimentally. This section is divided into two main parts. A theory subsection introduces the important quantities like group index N_g, Q and field enhancement factor η. These quantities are then used to derive expressions for the group delay experienced in the investigated WGGs. In the subsection 4.2 we calculate numerically a relation between the length of the grating and the quantities mentioned above. The simulations also demonstrate that the fringes in the transmission spectrum are related to resonances in the grating. In the experimental section 4.3 we will present the measured transmission and scatter data from a 500, 1000 and 2000 period WGG. The maximum values of Q, η, and N_g are obtained from these measurements. The delay times derived from the equations given in the theory section are compared with the group delays measured using the phase shift method.

4.1 Theory

In this section we will present the expressions that relate the group index to four different parameters of a resonator that can be directly measured: the Q factor, the scattered power, the free spectral range (FSR), and the group delay. In order to compare the methods experimentally, the first three parameters will be written as three separate expressions fro the delay times.

In general the group velocity describes the velocity at which envelope of a modulated optical signal is traveling. The modal group velocity can be calculated from the dispersion curve of an optical mode for an infinitely long grating using the following relation:

$$v_g(\omega) = \frac{d\omega}{dk}, \tag{1}$$

#78260 - $15.00 USD Received 20 December 2006; revised 8 February 2007; accepted 9 February 2007

with ω as the angular frequency and k defined as the wave vector ($2\pi/\lambda$) of the optical wave. The group index is defined as $N_g = c/v_g$. A resonance can be described by its quality factor Q defined as,

$$Q = \omega_0 \frac{U}{dU/dt}, \tag{2}$$

where U is the time averaged energy stored in a resonator at the resonant angular frequency ω_0, and (T_0 dU/dt) is the energy loss in one period T_0 ($=2\pi/\omega_0$) of this frequency. Assuming an exponential decay of the resonator with decay time $\tau_c = U/(dU/dt)$, it follows

$$Q = \omega_0 \tau_c. \tag{3}$$

A practical method for determining Q is by measuring the spectral transmission response of a resonator. The Q factor can than be obtained using the expression:

$$Q = \frac{\lambda_0}{\Delta\lambda_{-3\mathrm{dB}}}, \tag{4}$$

with $\Delta\lambda_{-3\mathrm{dB}}$ as the full width at half maximum of the Lorentzian shaped spectral response of the resonator and with λ_0 as the resonance wavelength.

In order to relate Q to the group velocity and to measurable scattered light, we will evaluate Eq. (2) using a power balance as illustrated by Fig. 3. To find a relation between the intensity at resonance and Q and v_g we first write the energy stored in the resonator as the product of the energy density W_r with the modal volume of the resonator V.

$$U = W_r V = W_r A_r L. \tag{5}$$

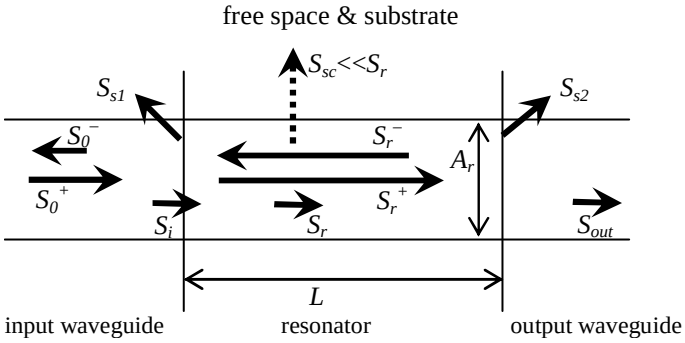

Fig. 3. Power balance of the resonator (effective length L, effective cross-section A_r) with input and output waveguides, and radiative coupling to free space (and substrate). The right traveling energy flux density S_0^+ in the input waveguide is partly back reflected (S_0^-) and couples in part to the resonator (flux density S_i) and in part to radiation modes S_{s1} due to modal mismatch between waveguide mode and resonator mode. Inside the resonator, the net flux density S_r , which is composed of a right traveling flux density S_r^+ and a left traveling one S_r^- is assumed to be constant along the cavity (neglecting S_{sc}). At the interface to the output waveguide, an output flux density S_{out} remains after subtracting radiation loss S_{s2} due to modal mismatch.

The volume of the resonator is formally written as the product of an assumed modal cross-sectional area A_r and the cavity length L. In a stationary state, the outgoing energy loss per period at the right hand side (S_{out}) is exactly equal to the energy flux fed to the resonator [36] (neglecting S_{sc}). Therefore the time derivative of U can be written as,

$$\frac{dU}{dt} = S_i A_r. \tag{6}$$

#78260 - $15.00 USD Received 20 December 2006; revised 8 February 2007; accepted 9 February 2007

Here, S_i is the net energy flux density (power density) that is transferred to the resonator. We assume the scattering loss from the cavity to be relatively small, so that the scatter flux S_{sc} is small compared to the net intensity flux inside the resonator S_r. Then S_r will be approximately constant and equal to S_i, and its relation to v_g is given by [11],

$$S_i \approx S_r = W_r \, v_g . \tag{7}$$

Next, we can write Q as a function of v_g at the resonance wavelength, by using Eqs.(2), (5), (6) and (7),

$$Q = \omega_0 \frac{W_r V}{S_r A_r} = \omega_0 \frac{S_r}{S_i} \frac{L}{v_g} = \omega_0 \frac{L}{v_g}. \tag{8}$$

Equation (8) can be rewritten as,

$$Q = 2\pi \frac{L \, N_g}{\lambda_0}. \tag{9}$$

The group index can be related to the group delay t_d of a resonator, which can be measured, for example as done in this paper, by using the phase shift method. This relationship is given by:

$$t_d(\lambda) = \frac{L}{c} N_g(\lambda). \tag{10}$$

An important observation can now be made by comparing Eqs. (9) and (10), and using (3): the group delay t_d of the resonator is equal to its cavity decay time τ_c, which was also derived in [36]. This relation can be understood from the fact that the group delay is determined by the response of the resonator (filter) within this exponential decay time. A group delay larger than the decay time would be unlikely, because the power has leaked away, leaving no power to support the signal further. Using Eq. (3) we define the delay (decay) time t_q derived from the measured Q [Eq. (4)] at the resonance wavelength as:

$$t_q = \tau_c = \frac{Q \lambda_0}{2\pi c}. \tag{11}$$

From Eq. (7) we can see that at a constant input power density S_i, a lower group velocity implies a higher energy density W_r. The ratio η between the average energy in the cavity at two different wavelengths λ and λ_{ref}, hence different group indices N_g and $N_{g,ref}$, can than be written as:

$$\eta(\lambda) = \frac{U}{U_{ref}} = \frac{W_r(\lambda) V}{W_{ref}(\lambda_{ref}) V} = \frac{S(\lambda) \; v_{g,ref}(\lambda_{ref})}{S_{ref}(\lambda_{ref}) \; v_g(\lambda)} = \frac{N_g(\lambda)}{N_{g,ref}(\lambda_{ref})}. \tag{12}$$

This equation allows us to calculate N_g at a specific wavelength λ, if both $N_{g,ref}$ is known, and η is known at wavelength λ. With the FScM approach we present a method for estimating the reference group index $N_{g,ref}$ in order to measure N_g at wavelengths near the band edge. The scattered power $I_{sc}(\lambda)$ is proportional to the probability that a photon is scattered, which is proportional to the number of photons in the resonator, hence to the total energy. This is true if the considered wavelength range is small (to limit the influence of the λ^{-4} dependency of Rayleigh scattering), the number of scatterers is high and the distribution is random, which is the case in our WGGs as can be observed further in this paper, in Fig. 9(b). We assume that in the wavelength region of interest, the scatter efficiency is not strongly wavelength dependent. By measuring a reference scatter intensity $I_{sc,ref}(\lambda_{ref})$ at a wavelength where a value for N_g is known (a method will be explained in section 4.2), an estimate for $N_g(\lambda)$ can be found:

#78260 - $15.00 USD Received 20 December 2006; revised 8 February 2007; accepted 9 February 2007

$$\eta(\lambda) = \frac{N_g(\lambda)}{N_{g,ref}(\lambda_{ref})} \approx \frac{I_{sc}(\lambda)}{I_{sc,ref}(\lambda_{ref})}. \tag{13}$$

An equivalent group delay t_{sc} can be calculated from the measured scatter ratio η by substituting (13) into (10):

$$t_{sc}(\lambda) = \frac{L}{c}\eta(\lambda)\, N_{g,ref}(\lambda_{ref}). \tag{14}$$

It is also possible to calculate Q from the scatter ratio (or visa versa) at the resonance wavelength λ_0, by substituting t_{sc} from (14) for t_q in (11):

$$Q(\lambda_0) = \eta(\lambda_0)\frac{2\pi\, L\, N_{g,ref}(\lambda_{ref})}{\lambda_0}. \tag{15}$$

In the derivations above, we assumed the equivalence of (group) delays that are measured or calculated in different ways at the resonance wavelength: directly measured, calculated from Q, and calculated from measured scatter enhancement η: $t_d \approx t_q \approx t_{sc}$.

A method, based on the Fabry-Perot free spectral range (FSR) equation, is sometimes applied [21, 22] to derive the group index from the transmission spectrum.

$$\Delta\lambda_{FSR} = \frac{\lambda_0^{\,2}}{2N_g\, L}. \tag{16}$$

Again using (10), one more equivalent group delay t_{FSR} can be found.

$$t_{FSR} = \frac{\lambda_0^{\,2}}{2c\,\Delta\lambda_{FSR}}. \tag{17}$$

Without further evaluating this expression, we will test this FSR-method for its validity by comparing its results with the other methods.

Finally we will derive a value for the group velocity applicable over the whole spectrum from the modeled complex transfer function to get more insight into the dispersion behavior of the WGG. It is well known that periodic structures can have a flat angular frequency vs. wavenumber (ω–k) dispersion curve for a small wavelength range close to the photonic band edge. For finite structures however, this curve never becomes completely flat, i.e. the group velocity will not approach to zero. The minimum v_g can be calculated using the complex optical transfer function $t(\omega)$ of the WGG [14]:

$$t(\omega) \equiv x(\omega) + \mathrm{i}\; y(\omega). \tag{18}$$

The group velocity of a propagating mode in the WGG can be determined by calculating $\mathrm{d}\omega/\mathrm{d}\varphi$, with φ defined as the total phase kL, with L the device length which equals the number of periods N times the period Λ. Using $\varphi = \tan^{-1}(y/x)$, the group velocity can be calculated from the (computed) real and imaginary parts of the transfer function, as follows [14]:

$$v_g = \frac{d\omega}{dk} = L\frac{x^2 + y^2}{x\dfrac{dy}{d\omega} - y\dfrac{dx}{d\omega}}. \tag{19}$$

4.2 Method & simulations

To study the properties of the WGGs grating resonances we used a bi-directional eigenmodes propagation method (BEP) [37] with 128 basis functions (eigenmodes) to calculate the complex transfer function $T(\omega)$ for TE polarization. The group index was derived as a function of the wavelength using Eq. (19), and the transmission of the WGG (T_g) is derived

#78260 - $15.00 USD Received 20 December 2006; revised 8 February 2007; accepted 9 February 2007

from the absolute value of the complex transfer function, see Fig. 4. We chose a WGG having a total number of periods of 350 instead of the fabricated 500 or more, for computing time/resources convenience. The group index shows two major peaks near the stopband edges of almost equal height/value. A maximum value for N_g = 7.3 at the smaller wavelength band edge is derived for this grating. Moving away from the band edge, the group index rapidly decreases to a value of ~1.86 (at 1560 nm) approximately equal to the N_g of the unperturbed ridge waveguide. This effect is used to define the reference group index ($N_{g,ref}$). At a wavelength around for example 1560 or 1510 nm, we can determine the scatter intensity, which we then relate to the reference scattering intensity $I_{sc,ref}$. However this approach is not used in this paper; we take the average of the oscillation present around these reference wavelengths. A value for the group index of the WGG can then be calculated using Eq. (13).

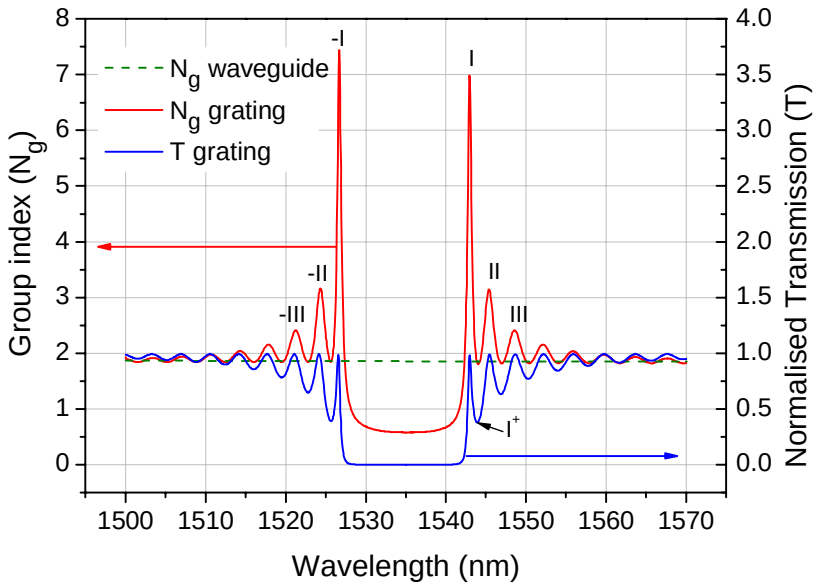

Fig. 4. The group index of a reference waveguide (dashed) and the normalized transmission T (blue) and group index (red) of a 350-period WGG obtained using a BEP method and Eq. (19).

For the weak or moderate grating strengths as in the modeled WGG displayed in Fig. 4, we observe approximately symmetric $T(\lambda)$ and $N_g(\lambda)$ curves [7]. A small difference can be seen between the group index curve shapes near the lower and upper wavelength edges. This is due to numerical errors in calculating the derivatives in (19); a larger number of simulation points will yield a more accurate result.

We note that the simulated WGG was modeled without optical loss due to absorption by the material or scattering, caused by inevitable errors in the fabrication processes. Consequently, the fringes in the fabricated WGGs (in Fig. 9) will be less narrow than in the simulated gratings. Imperfections such as variations of layer thickness and etch depth, will compromise the geometrical coherence of the structure, which will cause serious deviations from the calculated response for longer gratings. For larger fabrication errors or larger L the grating may act as an apodized grating. We found in our measurements (section 4.3) that for a maximum number of periods of 2000 (L ~ 1 mm), the WGG still showed the clearly separated fringes as seen in the simulations.

#78260 - $15.00 USD Received 20 December 2006; revised 8 February 2007; accepted 9 February 2007

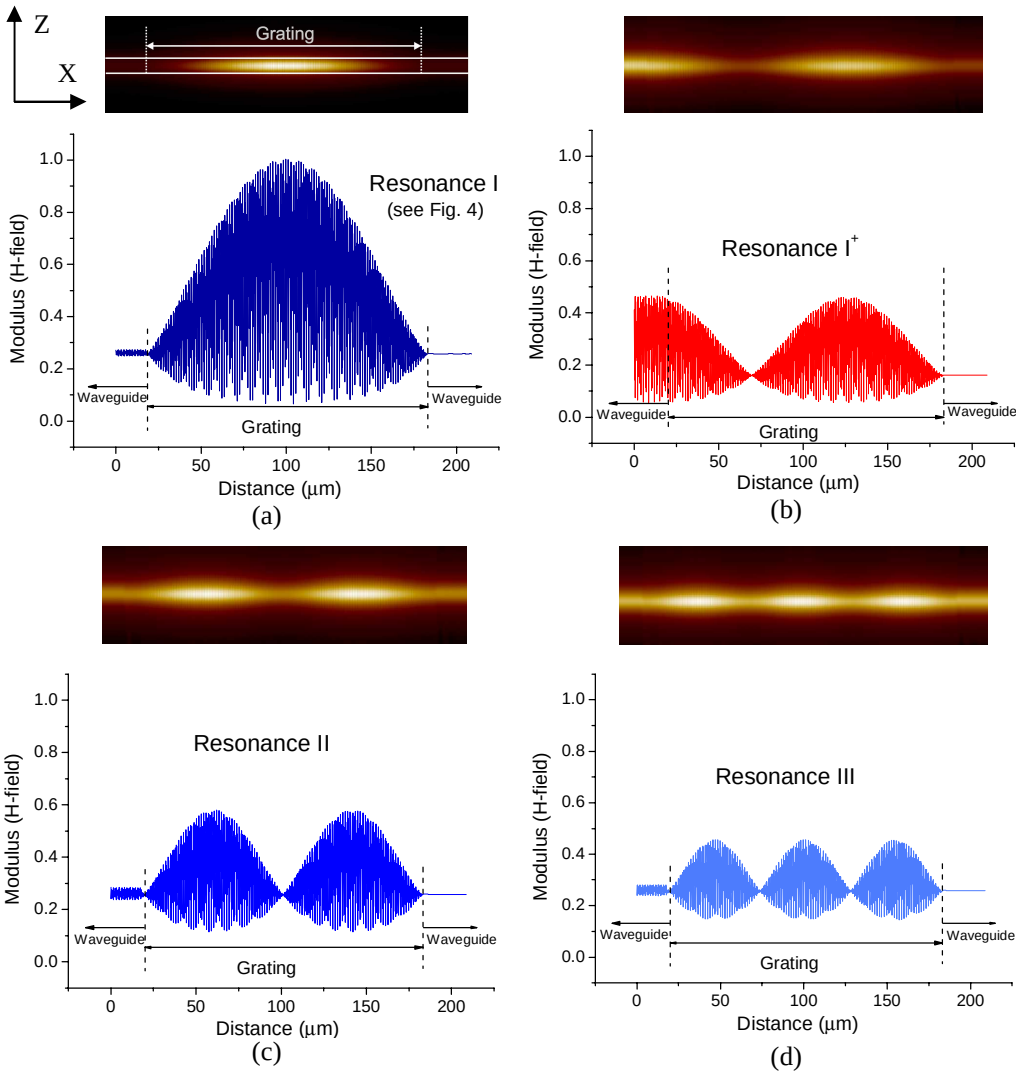

Fig. 5. Intra-cavity grating resonance modes in the dielectric band obtained via BEP Simulations. (a)-(d) The top image shows the H-field amplitude in the cross-section of the WGG for the resonance wavelengths shown in Fig. 4. The x- and z-coordinates are defined in Fig. 2. The bottom graphs show the H-field amplitude along the center-line of the guiding layer.

Besides the maximum N_g of a WGG, we can also find the longitudinal intra-cavity grating resonance patterns using the BEP method by modeling the cross-section of a WGG, see Fig. 5. These resonances are also verified experimentally in section 4.3 At the maximum of each fringe we can find a sinusoidal field distribution along the length of the grating, with nodes at its beginning and end; a simple mathematical derivation for this phenomenon can for example be found in Ref. [11]. The first resonance near the dielectric band edge, labeled as 'Resonance I' in Fig. 4, shows a single maximum exactly in the middle of the grating [Fig. 5(a)]. The top image shows the H-field distribution in the cross-section of the WGG. The lower plot shows the field distribution exactly in the middle of the Si_3N_4 slab. In the feeding waveguide (left) we see a small ripple indicating a small residual reflection. At the first minimum in the transmission curve, denoted by 'Resonance I^+' [Fig. 5(b)], a strong reflection is evidenced by the large amplitude of the standing wave in the input waveguide. At the start of the grating,

#78260 - $15.00 USD Received 20 December 2006; revised 8 February 2007; accepted 9 February 2007

we now find a maximum and inside the grating we find both a minimum and a maximum. On the output of the grating (right) we observe a lowered value of the transmitted field, which is consistent with the calculated transmission shown in Fig. 4. Increasing the wavelength further, away from the stop band, we find the higher order resonances. Figures 5(c) and 5(d) show the higher order resonances II and III. The maximum H-field amplitude decreases with the resonance order, which is expected from Fig. 4, which shows equivalently a decrease in group index. This decrease in modal-amplitude can be explained by the decrease in reflectivity from the grating for wavelengths further away from the Bragg condition.

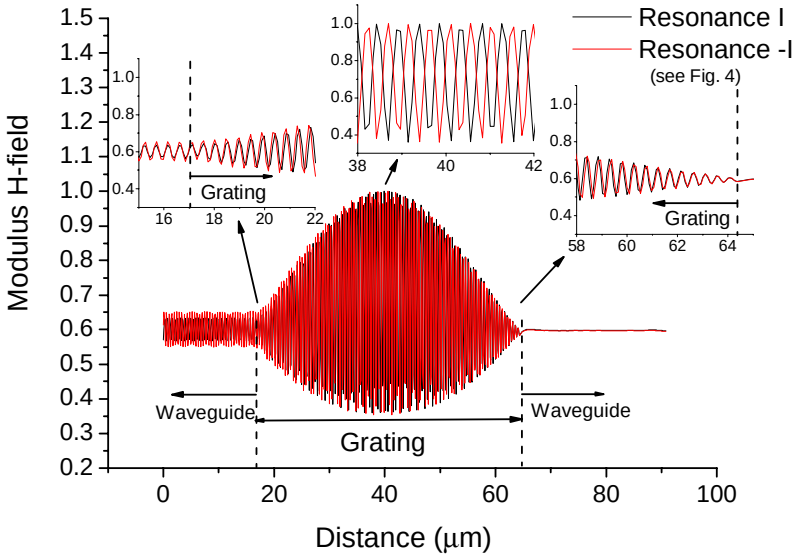

Fig. 6. Field amplitude (H-field) of the grating resonances at both band edges (resonances I and -I) of a 100-period WGG. In the middle section of the periodic medium (the grating) we see the well known phenomena [8] (studied by overlaying the grating structure with the field-distributions): the field for the first resonance in the air band is concentrated in the grooves (low-index) and for the dielectric band in the teeth (high-index). There is a shift between both field distributions of half a period. At the transition between the grating and the waveguide we observe the same (in phase) field distribution.

In Fig. 6, we have plotted both resonances near the band edge of the WGG in black and in red corresponding to Resonance I and –I (Fig. 4) respectively for a 100-period WGG. For a slow wave at the airband edge it is expected that the light is mainly concentrated in the low-index regions of the periodic medium [8]: the grooves of the grating, and for the dielectric band edge in the high index regions: the teeth of the WGG. These assumptions are based on an infinite structure using periodic (Bloch) boundary conditions. Figure 6 shows that for a finite structure, this is indeed the case for a region around the center of the periodic medium (the location of the field has been checked with the modeled WGG). However moving outwards, we find both field intensity distributions coinciding. The region where the field maxima are shifted by half a grating period can be increased by choosing a longer or stronger grating. The above phenomena can be explained, using the theory outlined in Ref. [12], in terms of the interference between the two counter propagating intra-cavity modes, for the wavelength regions above and below the band gap.

#78260 - $15.00 USD Received 20 December 2006; revised 8 February 2007; accepted 9 February 2007

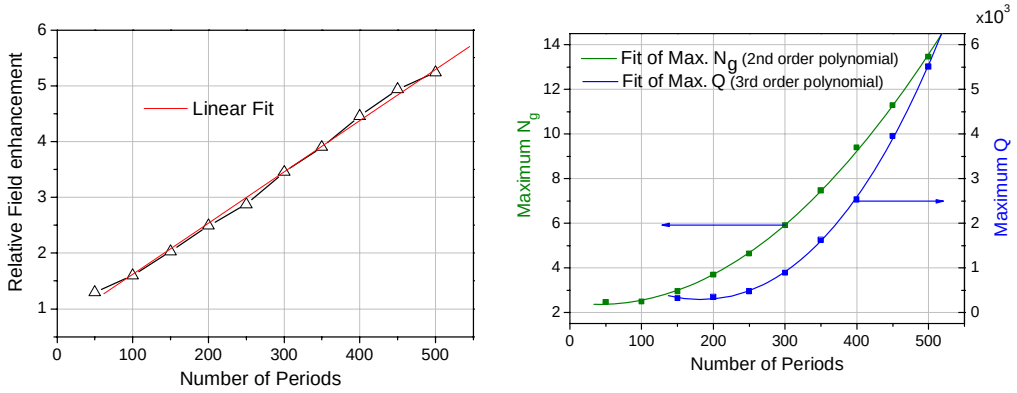

Fig. 7. (a). Maximum field strength as function of the number of periods. (b) Maximum group index (N_g) and Q versus the number of periods.

It has already been shown that the maximum field enhancement factor is linear with the length of the grating [38]. This is also verified by the modeling results presented in Fig. 7. Panel (a) shows the maximum relative field enhancement η found at the first resonance fringe (resonance I in Fig. 4) versus the number of periods, calculated using BEP modeling. The figure clearly shows the expected linear relationship. Besides the field enhancement, we also calculated the group index as a function of the number of periods. The curve for the maximum N_g (at resonance I) is quadratically related to the number of periods as expected, since N_g is proportional to the maximum (relative) intensity, which is proportional to the square of the electric field. The fringes are narrow near the stop band and thus have a high Q ($=\lambda/\Delta\lambda_{-3dB}$). Further away from the band edge the Q of each fringe declines (Fig. 4) until it can not be defined anymore (less than 3dB difference between the maximum and adjacent minimum).

A third-order relationship between Q and the grating length has been found using coupled mode equations for a waveguide grating suitable for second harmonic generation [5]. Moreover, this relation can also be deduced from Eq. (9) by using the quadratic relation between N_g and L. We have also verified this relation by rigorous BEP modeling [Fig. 7(b)]. For gratings shorter than 200-periods, we have estimated the Q from the left half side of the resonance I, taking $\Delta\lambda_{3dB}$ as 2 times the value found left from the resonance wavelength at the -3dB point.

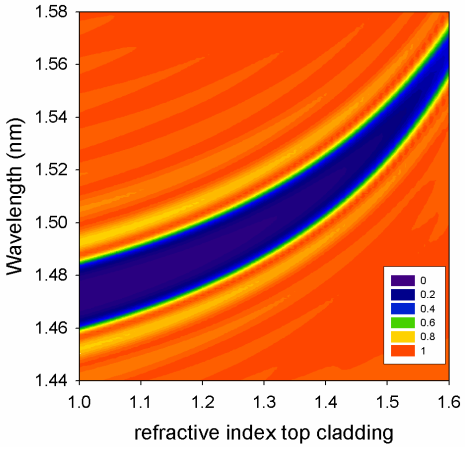

Fig. 8. Normalized transmission versus cladding index and wavelength for a 200-period WGG.

In the measurements presented in this paper, we have characterized WGGs with and without polymer cladding. Due to the higher contrast for the WGGs without cladding a higher maximum N_g is expected for the same device length. In Fig. 8 we have plotted the

#78260 - $15.00 USD Received 20 December 2006; revised 8 February 2007; accepted 9 February 2007

transmission as a function of the refractive index of the cladding and the wavelength for a 200-period WGG. The figure clearly shows how the stop band shifts with cladding index. As expected the stopband shifts to larger wavelengths when the refractive index of the cladding is increased.

4.3 Experimental

The transmission of the 500-period grating was measured after applying a polymer cladding with refractive index 1.5 onto the structure shown in Fig. 1(a), see Fig. 8 for location of the stop band as a function of the cladding index.

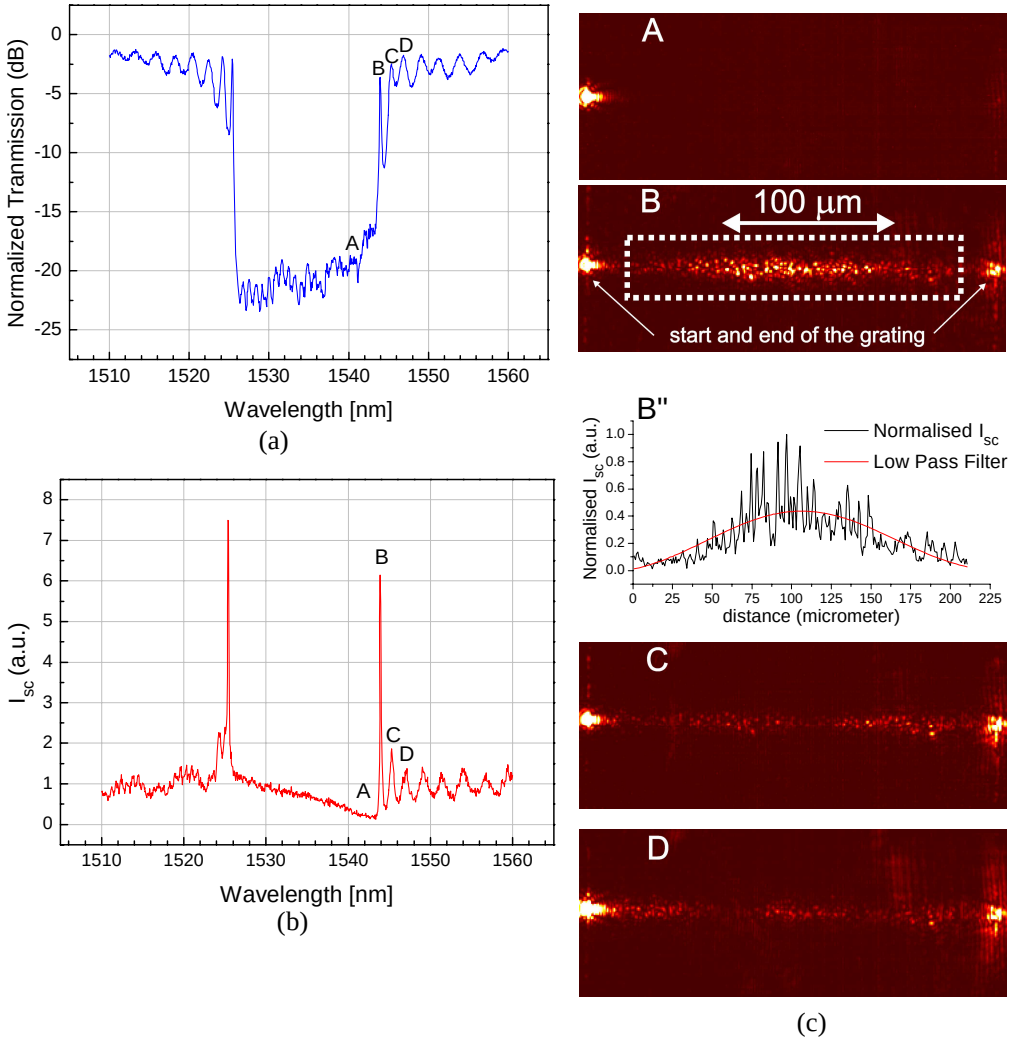

Fig. 9. Measurements on the 500-period waveguide grating. (a) Transmission spectrum of the WGG. (b) The scatter intensity (I_{sc}) collected using the NIR camera. (c) Scatter image A is taken from the grating region without cladding at the wavelength in the stopband labeled A in the transmission and scatter graphs (panels (a) and (b), respectively). A wavelength scaling factor has been used to account for the difference in cladding index, as explained further in the text. Only scattering from the input spot is observed for this wavelength. Image B is taken at the lowest-order resonance wavelength. The smoothed curve in graph B″ shows a single maximum. Images C and D show 2 and 3 intra-cavity maxima, respectively. The frames A to D can be clicked to start a movie (2.67 MB) of the transmission versus an increasing wavelength (6.82MB version).

#78260 - $15.00 USD Received 20 December 2006; revised 8 February 2007; accepted 9 February 2007

Next to the stopband, we find the predicted narrow fringes, see Fig. 9(a). The *Q*s of resonances I and –I (Fig. 4) are ~8500 and 6000, respectively.

To obtain clear images of the intensity distributions of the grating resonances we also captured the scattered light without the use of a polymer cladding. Due to the difference in cladding index, the spectra of the air-clad device were down-shifted by approximately 70 nm compared to the polymer-clad devices. This scaling has been taken into account for locating the labels A-D in Figs. 9(a) and 9(b).

Image A in Fig. 9(c) shows a capture for a wavelength in the stopband [see Fig. 9(a) or 9(b)] for the location in the spectrum). Only one bright spot is seen, which is the scattering from the transition of waveguide to WGG. Slightly increasing the wavelength to the first resonance in the dielectric band results in the single maximum intensity distribution shown in B (resonance I, Fig. 4). Graph B″ shows the scatter intensity (I_{sc}) integrated over a vertical line in the dotted box shown in B as a function of the distance (horizontal in the box). Although the camera images cannot resolve the sub-wavelength details of the field distribution in the grating area, they clearly show the envelope of the intensity distribution of the Fabry-Perot-like resonances of the Bloch modes in the WGG. By integrating I_{sc} over the area enclosed by the dotted box, it is possible to derive the I_{sc} spectrum shown in Fig. 9(b).

The maximum intensity enhancement (η) we obtain is about 7.4 taking the scattered intensity at 1514 nm as a reference. Using Eq. (13) and taking the reference index $N_{g,ref}$ equal to the group index of the undisturbed ridge waveguide ($N_{g,ref} \approx 1.9$) a value of $N_g \approx 7.4 \times N_{g,ref} = 14$ can be calculated. This corresponds to a group velocity of ~0.07 c. The estimated value of N_g using Eq. (9) with a Q of 8500 is about 8.8. The deviation between both numbers could be explained from the definition of Q given in Eq. (4). The shape of the fringes near the stop band is not strictly Lorentzian, because the reflectance changes rapidly with wavelength. Therefore, Q derived from the spectrum may be different from the actual Q value defined by Eq. (2) at the resonance wavelength.

In the experiments performed on the longer gratings, which will be discussed next, we notice that the deviation between both methods for obtaining the group index is smaller which may indicate that the *Q*s are more accurately determined using Eq. (9) for the longer gratings. Also other factors may contribute to small differences, for example the presence of slab-light and/or noise by the input and output spot of the WGG (see Fig. 9(c) image D), to which the FScM-method is sensitive. For longer WGGs the influence of both contributions is lower, which results in a better signal-to-noise ratio and a better agreement between both methods as we will show. The group delay can now also be calculated using Eq. (11) and Eq. (14), resulting in values $t_q \approx 7$ ps and $t_s \approx 11$ ps.

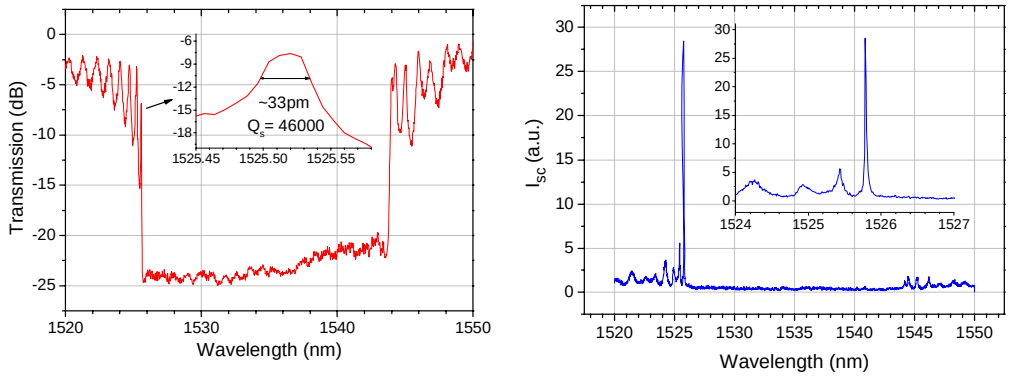

Fig. 10. Measurements on the 1000-period grating. (a) Transmission spectrum of the WGG, showing a very sharp fringe with a FWHM of only 33 pm in the airband, which corresponds to a Q of 46000. (b) The scatter intensity (I_{sc}) spectrum collected using the NIR camera.

#78260 - $15.00 USD Received 20 December 2006; revised 8 February 2007; accepted 9 February 2007

A larger value for N_g can be expected when the length of the selected WGG is increased [Fig. 7(b)] to 1000 periods. The measured transmission curve of this grating is shown in Fig. 10(a). The fringes in the airband are separately observable, whereas the fringes in the dielectric band show overlap near the edge, which is caused by fabrication errors inducing apodization, see Ref. [13] and the references therein. The first order resonance (resonance –I) shows a FWHM of only ~33 pm, which corresponds to a Q of 46000. Figure 10(b) shows the corresponding spectrum of the scattered intensity, from which a large $N_g \approx 24$ is deduced indeed at this high Q resonance, using Eq. (9). The noise level (due to slab light) in this particular grating was higher than in the other 2 gratings; therefore the background noise was subtracted from the scattered intensity collected from the grating area by selecting an equal sized area as reference next to the ridge waveguide at approximately 20 micrometer below the waveguide. From this scatter intensity enhancement we estimate η to be about 12. Using Eq. (13) we then find $N_g \approx 27$, corresponding to a group velocity of 0.04 c. For the corresponding group delays at the resonance wavelength (λ = 1525.52 nm) calculated using the measured Q and η, we find $t_q \approx 38$ ps and $t_{sc} \approx 42$ ps, respectively. Both methods agree quite well on the group index and consequently on the group delay at resonance –I (see Fig. 4).

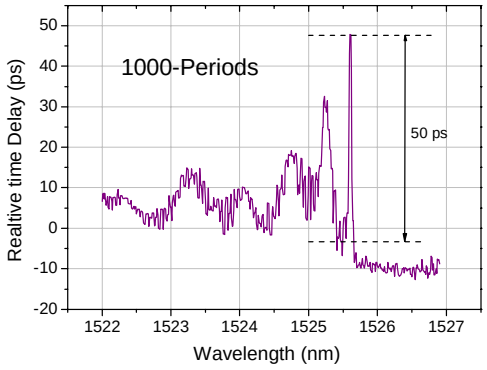

Fig. 11. Relative group delay as a function of wavelength, directly measured using the phase shift method for the 1000-periods long grating.

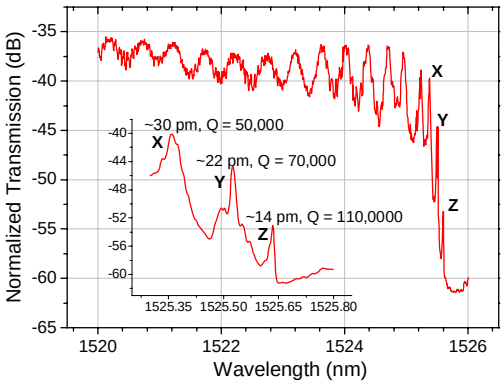

Fig. 12. Transmission spectrum obtained from the 2000-periods grating, zoomed in on the left edge.

However, with a reference measurement using the phase shift method to directly determine the group delay, a maximum $t_d \approx 50$ ps is found, see Fig. 11. The difference between t_q, t_{sc} and t_d can be explained from the inaccuracy in each method.

To compare the FScM method even further experimentally with the other methods, we doubled the number of periods again to 2000 resulting in a device length of 940 μm. The corresponding transmission spectrum is shown in Fig. 12, which is zoomed in on the air band region. For the resonances labeled *X*, *Y* and *Z*, Q-values of approximately 50 000, 70 000 and 110 000 respectively were found. With increasing Q the transmission drops due to the longer lifetime of the resonant photons, which causes a larger fraction of the light to scatter out of the WGG. The spectrum of the scattered intensity is shown in Fig. 13(a). We find a maximum $N_g \approx 25$ using Eq. (13), which results in a maximum group delay of $t_{sc} \approx 78$ ps [Eq. (14)]. For the maximum group delay calculated using the maximum Q of 110 000, a maximum $t_q \approx 88$ ps is found. The estimated group delays using both indirect methods match within 13%. The group delay calculated using the phase shift method is shown in Fig. 13(b). For resonance –I a maximum delay $t_d \approx 75$ ps is found. Although a larger N_g should be expected from a longer grating, the maximum N_g was found for the 1000-period grating, rather than for one with 2000 periods. Inaccuracies in the fabrication process limit the maximum achievable spatial coherence in the grating, which puts a limit on the maximum achievable Q.

#78260 - $15.00 USD Received 20 December 2006; revised 8 February 2007; accepted 9 February 2007

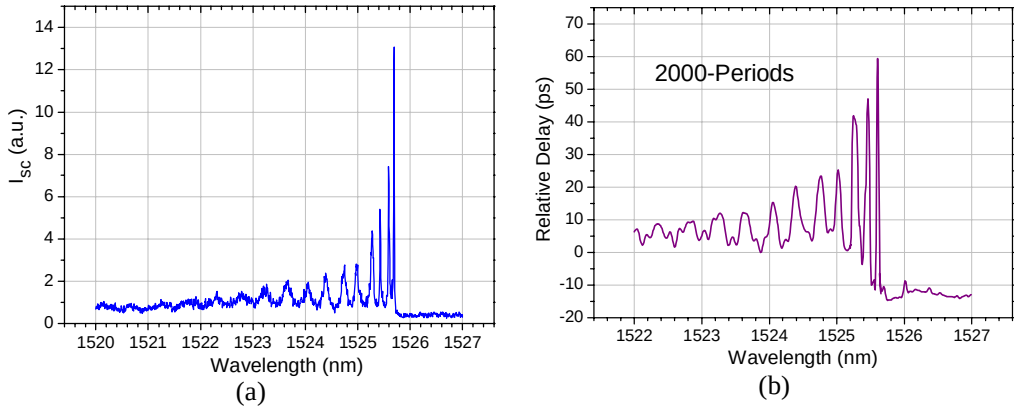

Fig. 13. Measurements on the 2000-periods long grating. (a) The scatter intensity spectrum (b) Relative group delay, directly measured using the phase shift method.

In the previous part we have focused only on the zero-order resonance in the airband (resonance –I), however the approach should also be valid for higher order resonances. To verify this we have determined several *Q*-values and plotted them as a function of η, see Fig. 14(a). The graph shows a linear relationship which agrees with Eq. (15).

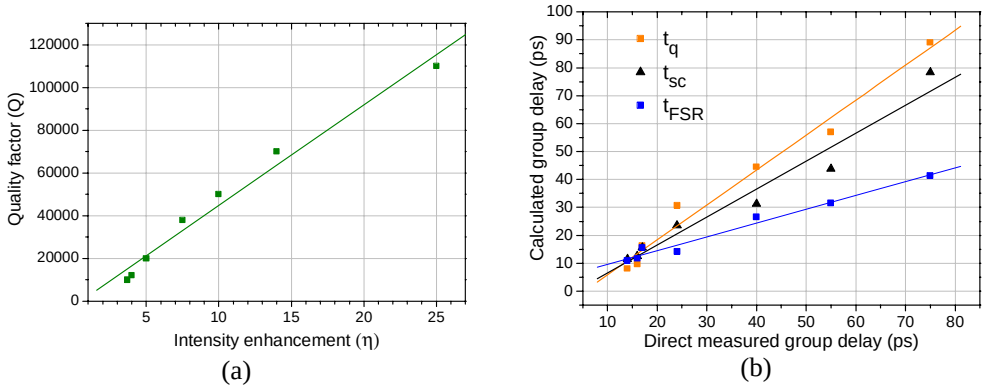

Fig. 14. (a). Experimentally derived relationship between η and *Q*. (b) Group delays calculated using various methods versus the directly measured group delay (t_d).

Figure 14(b) shows the indirectly derived group delays as a function of the directly measured time-delay. In this plot we also included the delay calculated from Eq. (17), using the FSR between the peaks. We observe that the group delays calculated from *Q* and η show a fairly good agreement with the directly measured group delay. From these results we can conclude that both indirect methods can be used to determine the group delay taking into account the accuracy of the methods.

Both methods are somewhat complementary; for example, a transmission spectrum, obtained using a high resolution tuneable laser having a small spectral linewidth, can be used for calibrating the FScM method. In this way N_g can be determined easily over a broad spectrum, by cancelling the noise contribution by slab light in the scatter experiments. On the other hand, the FScM method provides N_g also for wavelengths out of resonance. Figure 14(b) clearly shows that the FSR method [Eq. (17)] shows the strongest deviations from the values measured using the phase shift method, especially close to the band edge (at a t_d of 75 ps we find a t_{FSR} of ~40 ps). A possible explanation is the invalidity of the assumption of linear dispersion that is made to derive this equation (linear Taylor expansion), whereas in reality the dispersion curve is approximately quadratic near the stop band edge (ω versus β).

#78260 - $15.00 USD Received 20 December 2006; revised 8 February 2007; accepted 9 February 2007

5. Out of plane scattering

The coupling of period dielectric structures to input and output waveguides, mostly leads to an important source of loss in slab type designs, due to out-of-plane scattering (OPS). In order to optimize these transitions this loss needs to be analyzed. In section 5.1 we will briefly describe the origin and nature of the OPS, using BEP modeling. In section 5.2, we will show that the NIR camera allows us to determine the wavelength dependency of the OPS losses.

5.1 Simulations

The two main sources for out-of-plane scattering in the WGGs discussed in this paper are the scattering at the transition from waveguide to WGG and at the transition from WGG to waveguide, denoted as input and output spot respectively (see the images in Fig. 9). The scattering at the transition is caused by a modal mismatch between waveguide mode and the grating Bloch mode. Some adiabatic converters have been suggested for this transition [39, 40], but these tapers have the disadvantage of modifying the phase of the grating, which can lead to an apodized spectrum, which is clearly unwanted in this study.

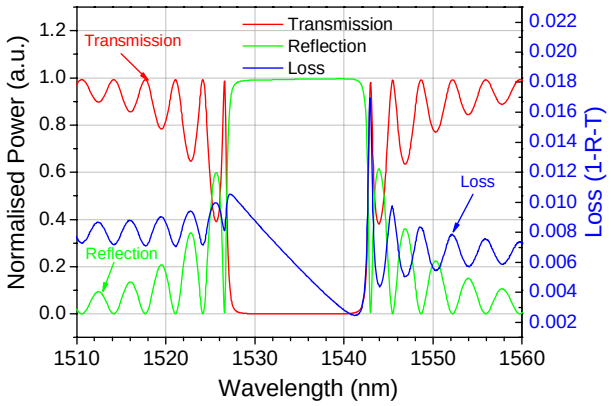

Fig. 15. A BEP [37] simulation of the transmission (*T*), reflection (*R*) and loss of a 350 period WGG. The out of plane loss is calculated using the relation OPS = 1 – *R* – *T*.

The result of a BEP simulation on a 350 period WGG is shown in Fig. 15. The same grating model as used for the results shown in Fig. 4 was chosen. The figure shows the transmission (*T*), reflection (*R*) and loss curves. The out of plane loss is calculated for each wavelength using the relation OPS = 1 – *T* – *R*. The loss-curve shows interesting behavior. It has a global minimum near the dielectric band edge, where the reflection reaches its maximum; for shorter wavelengths (in the bandgap) the loss increases and reaches a global maximum close to the air band edge. The loss maxima coincide with the transmission maxima in the dielectric band, whereas in the airband they coincide with the reflection maxima, a possible explanation will be given in the section below.

5.2 Experimental

In this paper we propose to quantify the out of plane loss by measuring the scattered light at the input and output of the grating. A figure for the OPS losses can be obtained by integrating the scatter data from the NIR camera over the input and output spot areas. Although our camera objective had a high NA (0.65), the OPS measured here may differ slightly from the actual OPS, because the scattering does not necessarily show a uniform distribution over all angles and over the complete spectrum analyzed here. However, it may provide relative information about the OPS. The scattering at both transitions can for example be compared. The sum of the OPS at both transitions may give a good figure for the behavior of the total OPS.

#78260 - $15.00 USD Received 20 December 2006; revised 8 February 2007; accepted 9 February 2007

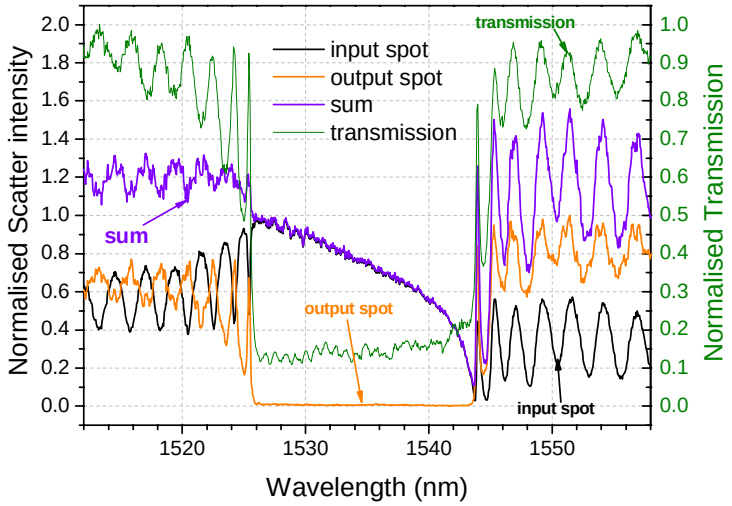

Fig. 16. Measurement of the scattering observed at the input and output spots of the grating. A sum of both gives a figure for the total OPS.

The OPS measurement results are presented in Fig. 16, which contains three curves, the measured (integrated) OPS from the input and output spot and the sum of both curves. We find that the OPS observed at the output spot is approximately proportional to the measured transmission of our structures. Some of the differences can be explained from the temperature drift (in the coupling conditions) in the two measurements, which were not performed at the same time.

Comparing the measured total OPS (the sum curve) with the OPS calculated using BEP simulation (Fig. 15) leads to the conclusion that both show resemblance. They both show a minimum in losses just before the first resonance in the dielectric band. Another agreement is found in dielectric and airband where in both cases the OPS loss has either coinciding maxima with the transmission curve (or output spot) or with the reflection (input spot). At wavelengths below the band edge the maxima in transmittance, and so in intra-cavity power, coincide with minima in the calculated loss curve (Fig. 15) and also with minima in the power scattered from a region near the input spot. This can be explained by assuming that, at the corresponding WG-WGG interface, light scattered by the two incoming modes (from left and right) is out of phase, leading to a cancellation of scattered power. This picture is supported by the observation from Fig. 16, that for wavelengths below the band-edge the dips in the power scattered at the input spot have approximately the same shape as the peaks in the transmittance. However some differences in shape and magnitude are observable apart from the high frequency ripples on the “sum” graph, for example in the stopband the shape differs from the simulated shape, most probably caused by fabrication inaccuracies. Nevertheless, we conclude that the NIR is also a powerful tool for investigating the relative OPS losses.

6. Sensor application

In this section we will discuss briefly an application for the high-*Q* gratings presented in this paper. Among many other applications, the relatively small, simple and easy to fabricate WGGs are suited for integration into sensor arrays. Their relatively small dimensions compared to linear phase based sensors, such as Mach-Zehnder Interferometers [41], allows for compact design while maintaining a high sensitivity [2]. The sensitivity can be calculated assuming a precision in minimum detectable change of transmission power of $\Delta T_0 = 10^{-4}$ (determined by the quality peripheral equipment and the number of samples taken) and the following approximation:

#78260 - $15.00 USD Received 20 December 2006; revised 8 February 2007; accepted 9 February 2007

$$\Delta n_{cladding} \approx \frac{\partial n}{\partial \lambda} \frac{\partial \lambda}{\partial T} \Delta T_0 \tag{20}$$

A value of ~15×10^{-12} can be estimated for $\partial\lambda/\partial T$ using the transmission curve in Fig. 12 (the 2000-period WGG, resonance *Z*). For $\partial n/\partial\lambda$ a value of 7.8×10^{6} m^{-1} (0.5 / 64 nm) is derived from the stopband shift with and polymer cladding, see also Fig. 8. Inserting these numbers in Eq. (20), we find a minimum detectable cladding index change $\Delta n_{cladding} \sim 1\times10^{-8}$. Such a grating sensor performs well compared to the state of the art MZI sensors ($\Delta n_{cladding} \sim 10^{-8}$) [41], especially when the size and simplicity are considered (for attaining the quoted sensitivity, the MZI sensor needs an advanced detection system). In conclusion we find that WGG gratings shown here are good candidates for all sorts of cladding sensors, for example: gas sensor without cladding or, for example, with a water-based cladding.

7. Conclusion

We have experimentally shown the existence of intensity resonance patterns in gratings which correspond well to the distributions found in the simulations of the waveguide grating. We have presented a novel and straightforward method for determining the group index and intensity enhancement over a wide wavelength range using the scatter intensity method. The far-field scattering microscopy method (FScM) was compared with two other methods and showed reasonable good agreement verifying the model presented in this paper. For the 500-period waveguide grating we found a minimum group velocity of 0.07 *c*. The 1000-period WGG showed a v_g as low as 0.04 *c*. For the 2000-period grating we measured a maximum *Q* of 110.000 and a maximum delay of 75 ps. The minimum v_g for this grating was estimated to be approximately equal to the value found for the 1000-period WGG: 0.04 *c*. The reason for this are the errors in fabrication.

In general we found that, the method estimating the group index (or delay) using the free-spectral-range formula (17) shows a significant deviation from the other methods, especially for the peaks at the stopband edge. In section 5 it was shown that the scatter data can also be used to analyze the out-of-plane scattering at the grating/waveguide transitions, which can be helpful for designing low insertion loss devices, for example. Finally we presented an application for the "high *Q*" WGG as compact sensor, and calculated the minimum detectable change in cladding index of 1×10^{-8}.

Acknowledgments

We thank Henry Kelderman, Henk van Wolferen their help with the laser interference lithography and Marco Gnan and Chris Roeloffzen for discussions. This work was supported by NanoNed, a national nanotechnology program coordinated by the Dutch ministry of Economic Affairs.